



# PUBLICATION

## MUSTANG

A MULTIPLE Space and Time scale Approach for the QUANTIFICATION of deep saline formations for CO<sub>2</sub> storage

**Project Number: 227286**

**AUTHORS:** Fuguo Tong, Auli Niemi, Zhibing Yang, Fritjof Fagerlund, Tobias Licha, Martin Sauter

**TITLE:** A Numerical Model of Tracer Transport in a Non-isothermal Two-Phase Flow System for CO<sub>2</sub> Geological Storage Characterization

The research leading to these results has received funding from the European Community's Seventh Framework Programme [FP7/2007/2013] under grant agreement n° [227286]

<b>Status</b>	AUTHOR VERSION
<b>Date</b>	2010
<b>Publisher</b>	Springer
<b>Reference</b>	Transport in Porous Media, Vol. 98, pp. 173-192

# A Numerical Model of Tracer Transport in a Non-isothermal Two-Phase Flow System for CO<sub>2</sub> Geological Storage Characterization

Fuguo Tong · Auli Niemi · Zhibing Yang ·  
Fritjof Fagerlund · Tobias Licha · Martin Sauter

Received: 25 June 2012 / Accepted: 2 February 2013 / Published online: 19 February 2013  
© The Author(s) 2013. This article is published with open access at Springerlink.com

**Abstract** For the purpose of characterizing geologically stored CO<sub>2</sub> including its phase partitioning and migration in deep saline formations, different types of tracers are being developed. Such tracers can be injected with CO<sub>2</sub> or water, and their partitioning and/or reactive transfer from one phase to another can give information on the interactions between the two fluid phases and the development of their interfacial area. Kinetic rock–water interactions and geochemical reactions during two-phase flow of CO<sub>2</sub> and brine have been incorporated in numerical simulators (e.g., Xu et al., TOUGHREACT User’s Guide: A Simulation Program for Non-isothermal Multiphase Reactive Geochemical Transport in Variably Saturated Geologic Media. LBNL Report 55460, V.1.2., Berkeley, CA, 2004). However, chemical equilibrium between the fluid phases is typically assumed, and multi-component, multiphase, non-isothermal codes for CO<sub>2</sub>–brine systems that incorporate kinetic mass transfer of tracers between the two fluid phases are not readily available. New models or further developments of existing models are therefore needed to provide the capability for interpreting the signals of novel tracers, including tracers with kinetic/time-dependent interface transfer. This paper presents such new numerical model of tracer transport in a non-isothermal two-phase flow system. The model consists of five different governing equations describing liquid phase (aqueous) flow, gas (CO<sub>2</sub>) flow, heat transport and the movement of the tracers within the two phases, as well as allowing kinetic transport of the tracers between the two phases. A finite element method is adopted for the spatial discretization and a finite difference approach is used for temporal discretization. Some special technologies and solution strategies are adopted for increasing the convergence, ensuring the numerical stability and eliminating non-physical oscillations. The new numerical model is validated against the code TOUGH2/ECO2N as well as some analytical/semi-analytical solutions. Good agreement between the simulated and analytical results indicates that the model has capability to simulate two-phase flow and

---

F. Tong (✉) · A. Niemi · Z. Yang · F. Fagerlund  
Department of Earth Sciences, Uppsala University, Villavägen 16, 75236 Uppsala, Sweden  
e-mail: fuguo.tong@geo.uu.se; tfg@ctgu.edu.cn

T. Licha · M. Sauter  
Department of Applied Geology, Geoscience Centre of the University of Göttingen, Goldschmidtstrasse  
3, 37077 Göttingen, Germany

tracer transport in a non-isothermal two-phase flow system with high confidence. Finally, the capability to model transport and kinetic mass transfer of tracers between the two fluid phases is demonstrated through examples.

**Keywords** Tracer transport · Two-phase flow · CO<sub>2</sub> geological storage · Numerical model · Finite element method

## 1 Introduction

Carbon dioxide (CO<sub>2</sub>) is the most important greenhouse gas, being responsible for over 60 % of the increase in the greenhouse effect (Kiehl and Trenberth 1997). It is widely recognized that an excess of carbon dioxide in the atmosphere increases the average temperature on the earth (e.g., Karl and Trenberth 2003). Geological storage of CO<sub>2</sub> allows injecting large volumes of CO<sub>2</sub> into the ground at sites suitable for geological storage (e.g., oil and gas reservoirs, unmineable coal seams, and deep saline reservoirs), and thus contributes to the mitigation of an increased greenhouse effect (Hepple and Benson 2004; Orr and Stanford 2004; Baines and Worden 2001). In order to ensure that the geologically stored CO<sub>2</sub> remains isolated from the atmosphere in the long term effective site characterization and monitoring techniques are needed and are also being developed.

Typically the storage formations are at depths of 800 to 3,000 m below ground surface and access to these formations is limited to a small number of deep boreholes. In addition, significant uncertainty in the geological properties and their spatial variation between the boreholes usually exists. Consequently, accurate monitoring of the spatial distribution of the injected CO<sub>2</sub> and its migration and fate is highly challenging. At the same time, in-situ information of CO<sub>2</sub> migration and trapping processes are crucial both in terms of improving our understanding of the fundamental phenomena as well as in commercial CO<sub>2</sub> storage projects, in which monitoring of the injected CO<sub>2</sub> is an important requirement. As a part of the EU-FP7 MUSTANG project (Niemi et al. 2012), different tracers are being developed and tested, specifically for the purpose of characterization of geologically stored CO<sub>2</sub> and its phase partitioning and migration in deep saline formations. These tracers include both more traditional partitioning tracers used in oil reservoir applications (e.g., Tomich et al. 1973) and CO<sub>2</sub> storage research (e.g., Zhang et al. 2011), and a set of novel reactive, kinetic interface-sensitive (KIS) tracers (Schaffer et al. in press; Licha et al. 2011; Behrens et al. 2006). Due to reactive processes at the CO<sub>2</sub>–brine interface, these tracers transfer from the CO<sub>2</sub> phase to the aqueous phase and thereby carry with them information about the CO<sub>2</sub>–brine active interfacial area, its development during the migration of the CO<sub>2</sub> plume. Hence they constitute a potentially powerful tool for in-situ CO<sub>2</sub> monitoring and research.

To correctly interpret the tracer signals, a numerical simulator which incorporates two-phase flow of CO<sub>2</sub> and brine as well as tracer transport and kinetic mass transfer of tracers between the two fluid phases is needed. Kinetic models have been developed for geochemical reactions and interactions between dissolved species in the aqueous phase and the solid phase (e.g., TOUGHREACT, Xu et al. 2004) during two-phase flow. However, commonly used two-phase flow and transport codes (Xu et al. 2004; Pruess et al. 1999; Pruess 2005; Hoteit and Firoozabadi 2008; Geiger et al. 2004; Helming 1997; Bear and Bachmat 1991; Aziz and Settari 1979) do not incorporate kinetic mass transfer between the two fluid phases. In this paper, a new numerical model is presented which incorporates kinetic reactions and kinetic tracer mass transfer from one fluid phase to the other in a non-isothermal two-phase flow system of CO<sub>2</sub> and brine. The model can be used to interpret tracer signals obtained from

field tests and subsequently aid the characterization of the geologically stored CO<sub>2</sub> including its phase partitioning and migration in deep saline formations.

The paper is organized as follows: First, we present the derivation of the governing equations for tracer transport in a non-isothermal two-phase flow system. The numerical discretization in space and time, and the solution strategies are introduced next (Sect. 3), followed by a discussion of the main constitutive models and parameters involved in the fourth section. Finally, the model verification against a semi-analytical solution and numerical simulations with the TOUGH2/ECO2N code (Pruess 2005) are presented along with model demonstration for the reactive tracer transfer over the phase interface.

## 2 Governing Equations

The medium is viewed as a mixed continuum of three independent overlapping phases where for every phase, their conservation equations can be obtained according to the principles of continuum mechanics (Bear and Bachmat 1991; Li et al. 1993). The general mass conservation equation for phase  $\alpha$  can be written as follows:

$$\partial_t(\rho_\alpha \phi^\alpha) + \nabla \cdot (\mathbf{v}_\alpha \rho_\alpha \phi^\alpha) - Q^\alpha = 0, \tag{1}$$

where  $\mathbf{v}_\alpha$ ,  $\rho_\alpha$ ,  $\phi^\alpha$ , and  $Q^\alpha$  are the velocity, the intrinsic density, the volume fractions, and the source of phase  $\alpha$ , respectively.

### 2.1 Aqueous Phase (Liquid) Flow Equation

The flow of the liquid (aqueous) phase is driven by gravity and the pressure gradient. The relative velocity of the liquid phase is expressed as:

$$\mathbf{v}_1^r = -\frac{k_1^r k}{\mu_1} (\nabla p_1 + \rho_1 \mathbf{g}), \tag{2}$$

where  $p_1$  is the pressure of the liquid phase,  $k$  is the intrinsic permeability,  $k_1^l$  is the relative permeability of liquid phase,  $\mu_1$  is the liquid viscosity,  $\mathbf{g}$  is the gravitational acceleration vector, and  $\rho_1$  is the liquid density. The relative velocity of the liquid phase can be expressed as:  $\mathbf{v}_1^r = \phi^l \mathbf{v}_1$ , where  $\phi^l$  is the liquid content. The velocity of the liquid phase ( $\mathbf{v}_1$ ) can then be written as:

$$\mathbf{v}_1 = \frac{1}{\phi^l} \left[ -\frac{k_r^l k}{\mu_1} (\nabla p_1 + \rho_1 \mathbf{g}) \right] \tag{3}$$

Substituting Eq. (3) as well as  $\phi^l = nS_1$  into Eq. (1), and then expanding, the following liquid flow equation is obtained:

$$\begin{aligned} nS_1 \frac{\partial \rho_1}{\partial t} + \rho_1 S_1 \frac{\partial n}{\partial t} + \rho_1 n \frac{\partial S_1}{\partial t} + \rho_1 \nabla \cdot \left[ -\frac{k_r^l k}{\mu_1} \cdot (\nabla p_1 + \rho_1 \mathbf{g}) \right] \\ + \rho_1 \left[ -\frac{k_r^l k}{\mu_1} \cdot (\nabla p_1 + \rho_1 \mathbf{g}) \right] \cdot \nabla \rho_1 - Q_1 = 0 \end{aligned} \tag{4}$$

Here,  $n$  is the porosity of porous medium and  $S_1$  is liquid saturation. In the case of the liquid phase being water, the density gradient ( $\nabla \rho$ ) is very small. Neglecting the smallest term:  $\rho_1 \left[ -\frac{k_r^l k}{\mu_1} \cdot (\nabla p_1 + \rho_1 \mathbf{g}) \right] \cdot \nabla \rho_1$ , and dividing by  $\rho_1$ , finally, the aqueous (liquid) phase flow

equation can be written as:

$$nS_1 \frac{\partial \ln \rho_l}{\partial t} + S_1 \frac{\partial n}{\partial t} + n \frac{\partial S_1}{\partial t} + \nabla \cdot \left[ -\frac{k_r^l k}{\mu_l} \cdot (\nabla p_l + \rho_l \mathbf{g}) \right] - \frac{1}{\rho_l} Q_l = 0. \tag{5}$$

### 2.2 Gas (CO<sub>2</sub>) Flow Equation

Similarly, the averaged advective velocity of gas phase (typically supercritical CO<sub>2</sub> in this study) with respect to the solid phase is driven by gravity and gas pressure, and is written as:

$$\mathbf{v}_g^r = -\frac{k_r^g k}{\mu_g} (\nabla p_g + \rho_g \mathbf{g}), \tag{6}$$

where  $\mu_g$ ,  $\rho_g$ ,  $k_r^g$  are the viscosity, density and relative permeability of the gas, respectively. The relative velocity of the gas phase can also be expressed as:  $\mathbf{v}_g^r = \phi^g \mathbf{v}_g$ , where  $\phi^g$  is gas content, and then the velocity of the gas phase ( $\mathbf{v}_g$ ) can be written as:

$$\mathbf{v}_g = \frac{1}{\phi^g} \left[ -\frac{k_r^g k}{\mu_g} (\nabla p_g + \rho_g \mathbf{g}) \right]. \tag{7}$$

Inserting Eq.(7) as well as  $\phi^g = n(1 - S_l)$  into Eq. (1), expanding and then dividing by  $\rho_g$ , the following equation for gas flow in porous media is obtained:

$$\begin{aligned} n(1 - S_l) \frac{\partial \ln \rho_g}{\partial t} + (1 - S_l) \frac{\partial n}{\partial t} - n \frac{\partial S_l}{\partial t} + \nabla \cdot \left[ -\frac{k_r^g k}{\mu_g} \cdot (\nabla p_g + \rho_g \mathbf{g}) \right] \\ + \left[ -\frac{k_r^g k}{\mu_g} \cdot (\nabla p_g + \rho_g \mathbf{g}) \right] \cdot \nabla \ln \rho_g - \frac{1}{\rho_g} Q_g = 0, \end{aligned} \tag{8}$$

where  $Q_g$  is the source term for the gas phase and other coefficients were defined previously.

### 2.3 Heat Transport Equation

The heat transport equation can be obtained based on the principle of thermal energy conservation. A detailed derivation was presented by Tong et al. (2010). The effects of deformation, thermal expansion (thermo-mechanical coupling between the solid, liquid and gas phases), and the effect of advection associated with the thermo-osmosis induced flow of the liquid and gas were ignored in the present analysis as they are not expected to be significant in tracer transport analyses. Basing the heat transport on heat conduction, heat capacity of the solid-fluid-gas system, and advective heat transfer associated with flow of liquid and gas, the final equation of heat transport can be simplified and expressed as:

$$\begin{aligned} \frac{\partial [(1 - n)\rho_s c_s T + nS_l \rho_l c_l T + n(1 - S_l)\rho_g c_g T]}{\partial t} - \nabla \cdot \left[ \rho_g c_g T \frac{k_r^g k}{\mu_g} (\nabla p_g + \rho_g \mathbf{g}) \right] \\ - \nabla \cdot \left[ \rho_l c_l T \frac{k_r^l k}{\mu_l} (\nabla p_l + \rho_l \mathbf{g}) \right] - \nabla \cdot (k_T \nabla T) - Q_T = 0. \end{aligned} \tag{9}$$

Here,  $\rho_s$  is the density of solid,  $c_s$ ,  $c_l$ ,  $c_g$  are the specific heat capacity of solid, liquid, and gas phase, respectively,  $k_T$  is the thermal conductivity, and  $Q_T$  is a heat source term.

### 2.4 Tracer Transport Equation

In field experiments on CO<sub>2</sub> transport and trapping in brine aquifers, tracers can be injected into the aqueous or the gas (supercritical CO<sub>2</sub>) phase and their evolution in the two phases can be used as an indicator of partitioning between the phases.

In this study, we are especially focusing on a case where tracers are injected with the gas phase (supercritical CO<sub>2</sub>), and their concentration in the liquid (water) is measured at later times. Therefore, it is necessary to distinguish between the tracer concentrations in gas and liquid phases. Here two independent variables of tracer concentration are needed (the concentration of tracer in gas ( $C_g$ ) and the concentration of tracer in liquid ( $C_l$ )), and the movement of tracers in the gas and the movement of tracers in the liquid need to be described by their respective governing equations.

#### 2.4.1 Transport Equation of Tracer in Gas (CO<sub>2</sub>)

Mass conservation, described by Eq. (1), can be used as basis also when developing the governing equations for tracer transport. If the concentration of tracer in the gas phase ( $C_g$ ) is defined as the total mass of the tracer in gas divided by the total mass of gas in a unit volume, the first term in Eq. (1) can be expanded as:

$$\partial_t [C_g \rho_g \phi^g] = n(1 - S_l) \rho_g \frac{\partial C_g}{\partial t} + n(1 - S_l) C_g \frac{\partial \rho_g}{\partial t} + (1 - S_l) \rho_g C_g \frac{\partial n}{\partial t} - \rho_g C_g n \frac{\partial S_l}{\partial t}. \tag{10}$$

The movement of tracer in the gas phase includes diffusion and advection associated with gas flow. Then the real velocity of tracer in the gas phase can be expressed as:

$$v_{t-g} = \frac{1}{\phi^g} \left[ -\frac{k_r^g k}{\mu_g} \cdot (\nabla p_g + \rho_g \mathbf{g}) - D_g \nabla C_g \right], \tag{11}$$

where  $D_g$  is the dispersion coefficient for the tracer in the gas phase which includes the summed effects of mechanical dispersion and molecular diffusion.

Then the second item of Eq. (1) can be expanded as:

$$\begin{aligned} \nabla [v_{t-g} C_g \rho_g \phi^g] &= \rho_g C_g \nabla \cdot \left[ -\frac{k_r^g k}{\mu_g} \cdot (\nabla p_g + \rho_g \mathbf{g}) \right] + C_g \left[ -\frac{k_r^g k}{\mu_g} \cdot (\nabla p_g + \rho_g \mathbf{g}) \right] \cdot \nabla \rho_g \\ &+ \rho_g \left[ -\frac{k_r^g k}{\mu_g} \cdot (\nabla p_g + \rho_g \mathbf{g}) - D_g \nabla C_g \right] \cdot \nabla C_g + \rho_g C_g \nabla \cdot [-D_g \nabla C_g] \\ &+ C_g [-D_g \nabla C_g] \cdot \nabla \rho_g. \end{aligned} \tag{12}$$

Substituting Eqs. (11) and (12) into Eq. (1) while taking into account the mass conservation of gas flow (Eq. 8), the following transport equation for tracer in the gas phase is obtained:

$$\begin{aligned} n(1 - S_l) \rho_g \frac{\partial C_g}{\partial t} + \rho_g \left[ -\frac{k_r^g k}{\mu_g} \cdot (\nabla p_g + \rho_g \mathbf{g}) \right] \cdot \nabla C_g + \nabla \cdot [-(\rho_g C_g) D_g \nabla C_g] \\ + C_g Q_g - Q_{t-g} = 0. \end{aligned} \tag{13}$$

The source term for tracer in the gas phase,  $Q_{t-g}$ , is used to express the amount of tracer that is transferred from the CO<sub>2</sub> phase to the aqueous phase. Therefore, it is a critical function in the simulation of kinetic tracer transport between the two fluid phases.

### 2.4.2 Transport Equation of Tracer in Liquid (Water)

The concentration of the tracer in the liquid phase ( $C_1$ ) is defined as the total mass of the tracer in the liquid divided by the total mass of liquid in a unit volume. Then, similarly to the derivation of the transport equation for tracer in the gas phase, the transport equation for tracer in the liquid phase can be obtained and written as:

$$nS_1\rho_1 \frac{\partial C_1}{\partial t} + \rho_1 \left[ -\frac{k_r^l k}{\mu_1} \cdot (\nabla p_1 + \rho_1 \mathbf{g}) \right] \cdot \nabla C_1 + \nabla \cdot [-(\rho_1 C_1) D_1 \nabla C_1] + C_1 Q_1 - Q_{t-1} = 0, \tag{14}$$

where  $D_1$  is dispersion coefficient in the liquid phase, which represents the summed effects of mechanical dispersion and molecular diffusion, and  $Q_{t-1}$  is the source term for tracer in the liquid phase. Typically  $Q_{t-1}$  is used to express the amount of tracer that transfers from the aqueous phase to the  $CO_2$  phase, and thus it is equal to  $Q_{t-g}$  in magnitude, but with opposite sign. The model for tracer transfer between the  $CO_2$  and aqueous phases is defined in Sect. 3.5 Besides temperature and other factors, the rate of tracer mass transfer is also a function of specific fluid–fluid interfacial area; therefore, the tracer concentration gives information on the development of the interfacial area between the  $CO_2$ –brine, which plays a key role in this research.

## 3 Main Constitutive Models and Parameters

### 3.1 Characteristic Curves

There are a number of relationships describing the relationship between capillary pressure and phase saturation as well as phase permeability and phase saturation (e.g., Brooks and Corey 1964; Mualem 1976; Van Genuchten 1980; Jury et al. 1991; Bachmann and van der Plog 2002), some of which take into account the hysteretic characteristics of these functions. In the preliminary simulations presented in this paper, we neglect effects of hysteresis and use the well-known Van Genuchten (1980) model for capillary pressure,  $p_c$ , which can be expressed as:

$$p_c = -p_0 \left[ \left( \frac{s_1 - s_{1r}}{1 - s_{1r}} \right)^{-\frac{1}{\lambda}} - 1 \right]^{1-\lambda}. \tag{15}$$

For relative permeability to liquid, we use the Van Genuchten (1980)–Mualem (1976) model:

$$k_r^l = \sqrt{\frac{s_1 - s_{1r}}{1 - s_{1r}}} \left\{ 1 - \left[ 1 - \left( \frac{s_1 - s_{1r}}{1 - s_{1r}} \right)^{\frac{1}{\lambda}} \right]^\lambda \right\}^2. \tag{16}$$

Finally, we express the relative permeability to gas using the model by Corey (1954):

$$k_r^g = \left( 1 - \frac{s_1 - s_{1r}}{1 - s_{1r} - s_{gr}} \right)^2 \left[ 1 - \left( \frac{s_1 - s_{1r}}{1 - s_{1r} - s_{gr}} \right)^2 \right]. \tag{17}$$

### 3.2 Density

Density of water is defined as a function of temperature and pressure. It is calculated according to IAPWS (1994), issued by the International Association for the Properties of Water and

Steam (IAPWS). Considering that the change in water density usually is very small, in the present model, a simplified formula is adopted (Tong et al. 2010), expressed as:

$$\rho_l = \frac{K_1 \rho_T}{K_1 - p_l + 1.01325}, \tag{18}$$

where  $\rho_T = 1000.066219 + 0.0209229T - 0.00602137T^2 + 0.0000163T^3$  is the density of water at atmospheric pressure, in units of  $\text{kg/m}^3$ ,  $T$  is the temperature in  $^\circ\text{C}$ , and  $K_1 (= 2.15 \times 10^4 \text{ bar})$  is the bulk modulus of water.

The density of carbon dioxide is based on its equation of state as presented by Sterner and Pitzer (1994), applicable for temperatures from 215 to 2,000 K and for pressures from zero to over 10 GPa. For a given temperature and pressure, the equation of state of  $\text{CO}_2$  can be simplified as a nonlinear function of the density of  $\text{CO}_2$ . Thereby, it can be directly solved in the presented model using the so-called dichotomy method by Allen and Isaacson (1997), which is a method for numerical solution of equations in a single unknown.

### 3.3 Viscosity

The dynamic viscosity of water used in the model is based on the following equation by Guvanasen and Chan (2000):

$$\mu_l = 1.984 \times 10^{-6} \exp[1825.85 / (273 + T)], \tag{19}$$

where viscosity is in units of  $\text{Ns/m}^2$ .

For the dynamic viscosity of  $\text{CO}_2$ , we use the model utilized in the TOUGH2 simulator (Pruess et al. 1999; Battistelli et al. 1997), where viscosity of  $\text{CO}_2$  is a function of pressure and temperature and calculated using the correlation quoted by Pritchett et al. (1981). This formula is based on data tabulated by Vargaftik (1975).

### 3.4 Dissolution of Carbon Dioxide

The dissolution of carbon dioxide in pure water and sodium chloride brines is described using Henry’s law and the concept of salting-out is described following Battistelli et al. (1997). The concentration of carbon dioxide (in units:  $\text{kg/m}^3$ ) dissolved in water is a function of salt concentration and is expressed as follows:

$$C_{\text{CO}_2} = \frac{44}{18} \times \frac{P_{\text{CO}_2}}{(K_h \times 10^m K_b)}. \tag{20}$$

Here,  $P_{\text{CO}_2}$  is the pressure of  $\text{CO}_2$  in units of Pa,  $K_b$  is the salting-out coefficient, and  $m$  is salt molality.  $K_h$  is Henry’s constant for pure water (in units: Pa), and can be calculated as follows by a polynomial fit:  $K_h = \sum_{i=0}^5 B(i)T^i$  (Cramer 1982). Here,  $T$  is temperature, and the coefficients  $B(i)$  have the following values:  $B(0) = 78.3666$ ,  $B(1) = 1.96025$ ,  $B(2) = 8.20574 \times 10^{-2}$ ,  $B(3) = -7.40974 \times 10^{-4}$ ,  $B(4) = 2.1838 \times 10^{-6}$ ,  $B(5) = -2.20999 \times 10^{-9}$ . The salting-out coefficient is expressed as:  $K_b = \sum_{i=0}^4 C(i)T^i$ , where the coefficients  $C(i)$  have the following values:  $C(0) = 0.119784$ ,  $C(1) = -7.17823 \times 10^{-4}$ ,  $C(2) = 4.93854 \times 10^{-6}$ ,  $C(3) = -1.03826 \times 10^{-8}$ ,  $C(4) = 1.08233 \times 10^{-11}$ .

### 3.5 Tracer Transfer Between Liquid and Gas Phases

The key novelty of the numerical model presented in this paper is its ability to allow kinetic transfer of the tracer from one phase to another. Different models can be incorporated depending on the characteristics of the specific tracer in question. In the present demonstration, we



consider a tracer for which the rate of mass transfer from the CO<sub>2</sub> to the aqueous phase follows the model by [Miller et al. \(1990\)](#):

$$Q_{t-g} = -Q_{t-l} = k_1 a_{na} (C_s - C_l). \quad (21)$$

Here  $Q_{t-g}$  and  $Q_{t-l}$  are the source terms for tracer in the gas and liquid phases, respectively,  $k_1$  is the average mass transfer coefficient, and  $a_{na}$  is the specific interfacial area between the two fluid phases (specific here means area per unit volume of porous media). The specific interfacial area is a complex parameter in the case of porous media, but approaches for determining it from porous media data have been proposed, e.g., by [Grant and Gerhard \(2007a\)](#).  $C_l$  is the molar concentration of tracer in liquid, and  $C_s$  is the molar concentration of tracer in liquid that corresponds to the condition of thermodynamic equilibrium with the gas phase. In the case of chemically reactive tracers which undergo hydrolysis at the gas liquid interface,  $C_s$  can be calculated with the following formula ([Licha et al. 2011](#)):

$$C_s = C_g k_a = C_g A \cdot \text{Exp} \left[ -\frac{E_a}{R(273 + T)} \right], \quad (22)$$

where  $C_g$  is the molar concentration of tracer in gas,  $k_a$  is the mass flux constant of the tracer (in this case the zero order rate constant which combines mass transfer to, across and away from the interface with the hydrolysis rate constant of the involved reaction at the interface),  $A$  and  $E_a$  are the pre-exponential factor and activation energy for the specific hydrolysis reaction, respectively,  $R$  is the universal gas constant, and  $T$  is temperature at the gas/liquid interface in °C. This specific approach extends common tracer methods (based on simple partitioning) by including the rate of a chemical reaction at the fluid–fluid interface and thus incorporates true kinetically controlled mass transfer from one phase to the other. This new model allows a preliminary assessment of the potential of such kinetic interface-sensitive tracers which constitute a novel investigation tool in multiphase flow applications ([Schaffer et al. in press](#)).

## 4 Numerical Discretization and Solution Strategy

### 4.1 Numerical Discretization

#### 4.1.1 Spatial Discretization

The governing equations (5), (8), (9), (13), and (14) are nonlinear differential equations. To solve them, they must be appropriately discretized in space and time. A Galerkin finite element solution approach ([Zienkiewicz and Taylor 2000](#)) is used for the spatial discretization of Eqs. (5), (8), and (9). But for equations (13) and (14), the standard Galerkin method, in which interpolation functions themselves serve as weighting functions, cannot be directly used because this will generate numerical solutions with artificial and non-physical oscillations ([Younes and Ackerer 2005](#)). In the present numerical model, interpolation functions are linear function of space. In order to ensure local mass conservation, for a given Gauss integration point, the weighting functions of a node are set to zero when the gas (or water) pressure of the node is higher than the gas (or water) pressure of the Gauss integration point, and the sum of other nodes is equal to 1. Simulations show that this method performs well for eliminating any non-physical oscillations, thereby obeying local mass conservation and providing sufficiently accurate results.

When simulating CO<sub>2</sub> injection (migration of CO<sub>2</sub> in a brine aquifer), the first order derivative of water saturation with respect to the spatial coordinates is not continuous in the non-wetting phase (CO<sub>2</sub>) front if the initial degree of water saturation is 1.0. Therefore, some numerical oscillations will occur if the interpolation functions themselves serve as weighting functions for spatial discretization (Helming 1997). One of methods adopted in this numerical model to eliminate the numerical oscillations is to set the weighting functions as constants. The numerical aspects of this model, developed for best computational performance, are further discussed in Tong et al. (2012).

#### 4.1.2 Temporal Discretization

Within each time step, the primary variables are assumed to follow linear variations with time. For example, the degree of saturation (*S*) is assumed to be a linear function of time, and can be expressed as:

$$S = N_1 S^{t_k} + N_2 S^{t_k + \Delta t}, \tag{23}$$

where  $N_1 = 1 - \eta$ ,  $N_2 = \eta$ , and  $\eta = (t - t_k)/\Delta t$ ,  $t$  is the time, and  $\Delta t$  is the length of each time step. The parameter  $\eta$  may take any value from 0 to 1, to generate different finite difference method (FDM) schemes. The values of  $\eta = 0$ ,  $\eta = 0.5$ , and  $\eta = 1$  correspond to the three standard FDM schemes, i.e., forward difference (Euler), central-difference (Crank–Nicholson) and backward difference. In this numerical model, the value of  $\eta$  is 0.667, which corresponds to the Galerkin finite difference scheme.

#### 4.2 Solution Strategies

To solve these nonlinear governing equations, convergence, numerical stability and computational efficiency are always the three key components in the numerical solution. When solving the above Eqs. (5), (8), (9), (13), and (14), the Eqs. (5) and (8) are strongly coupled and need to be solved iteratively, while the heat transport and tracer transport equations are relatively independent, at least in this preliminary application, and are therefore not solved simultaneously. The general route for iterative solution is to calculate the two-phase flow equations first, after which the temperature is obtained by solving heat transport equation, followed by solving the tracer transport equations.

For the solution of the two-phase flow equations, gas pressure and water saturation are chosen as primary variables. In order to improve the convergence, Eqs. (5) and (8) are added together to eliminate the item  $n \frac{\partial S_1}{\partial t}$ , yielding the following equation for total mass conservation:

$$\begin{aligned} n(1 - S_1) \frac{\partial \ln \rho_g}{\partial t} + n S_1 \frac{\partial \ln \rho_l}{\partial t} + \frac{\partial n}{\partial t} + \nabla \left[ -\frac{k_r^g k}{\mu_g} \cdot (\nabla p_g + \rho_g \mathbf{g}) \right] \\ + \nabla \left[ -\frac{k_r^l k}{\mu_l} \cdot (\nabla p_g + \rho_l \mathbf{g}) \right] - \nabla \left[ -\frac{k_r^l k}{\mu_l} \cdot \nabla p_c \right] \\ + \left[ -\frac{k_r^g k}{\mu_g} \cdot (\nabla p_g + \rho_g \mathbf{g}) \right] \cdot \nabla \ln \rho_g - \frac{1}{\rho_g} Q_g - \frac{1}{\rho_l} Q_l = 0, \end{aligned} \tag{24}$$

where  $p_c$  is capillary pressure, defined as  $p_g - p_l$ . In Eq. (24), the coefficient of gas pressure is significantly bigger than that of water saturation. In this model, gas pressure and water saturation are calculated by solving Eqs. (24) and (8), instead of solving Eqs. (5) and (8)

together, for improving convergence and numerical stability. Moreover, Eqs. (24) and (8) are still valid even in the case of single phase flow.

Besides the route of solving Eqs. (8) and (24) together, another available iterative route is to first calculate gas pressure by solving Eq. (24) and then calculate the water saturation by solving Eq. (8). This circulating iteration will be kept until the values of gas pressure and water saturation do not change in a given time step. Because the water saturation is mainly related to gas pressure in Eq. (8), and capillary pressure does not appear in Eq. (8), the numerical stability of solving Eq. (8) is better than that of solving Eq. (5). In the examples presented in this paper, the number of iterations is limited to 5 and the convergence criterion is a relative error for gas saturation of less than 0.0001 in every time step. Calculations show that the above described iterative method has a good convergence behavior and numerical stability.

## 5 Model Verification and Demonstration

The verification of the developed numerical model includes three parts. The first part concerns the validation of the heat transport, which was presented by Tong et al. (2009, 2010), and is not repeated here. The second part is the verification of two-phase flow model, which is presented through comparisons against a semi-analytical solution and against numerical simulation results obtained with the TOUGH2/ECO2N model (Pruess 2005). The third part is a comparison between simulated and analytical results for the validation of tracer transport.

### 5.1 Conceptual and Numerical Model

In the verification and demonstration simulations, we consider CO<sub>2</sub> injection into a brine aquifer, where CO<sub>2</sub> is spreading laterally and rising upwards due to buoyancy. A two-dimensional vertical cross-section representing the reservoir layer, where CO<sub>2</sub> is being injected has properties as summarized in Table 1. The permeable reservoir layer is bound above and below by impermeable layers and the injection takes place over the entire 10-m thickness of the reservoir. Tracer is injected in the CO<sub>2</sub> phase and its concentration in the CO<sub>2</sub> and in the brine is monitored over time. The initial and boundary conditions are summarized in Table 2.

Quadrilateral elements are used to discretize the 100 m × 10 m model. After a grid convergence test with different element sizes, the final calculation mesh consists of a total of 2,000 elements and 2,112 nodes.

**Table 1** Material properties of the reservoir layer

Permeability	$1.0 \times 10^{-13}$
Porosity	0.15
Capillary pressure	Eq. (15) with $p_0 = 0.133$ bar, $\lambda = 0.4118$
Relative permeability of liquid	Eq. (16) with $s_{lr} = 0.3$ , $\lambda = 0.4118$
Relative permeability of gas	Eq. (17) with $s_{lr} = 0.3$ , $s_{lg} = 0.05$
Thermal conductivity	$1.28 - 0.71/[1 + \exp(10S - 6.5)]$
The kinetic transfer of the tracers between CO <sub>2</sub> and liquid water	Eqs. (21) and (22) with $k_1 = 6.8 \times 10^{-7}$ , $a_{na} = 154.8 \times (1 - S)$ , $A = 2.02 \times 10^{13}$ , $E_a = 90.0$ , $R = 0.008314$

**Table 2** Initial conditions and boundary conditions

Initial conditions	CO <sub>2</sub> pressure	15.6 MPa
	Temperature	50°C
	Water saturation	1.0
	Tracer in CO <sub>2</sub>	0.52 mol/kg
	Tracer in liquid	0.0
Boundary conditions	Gas flow equation, Eq. (8)	Left side: A given CO <sub>2</sub> injection rate ( $1.0 \times 10^{-5}$ m/s or $2.71 \times 10^{-6}$ m/s)
	Total mass equation, Eq. (24)	Right side: $P_g = 15.6$ MPa Above and below side: Impermeable Above and below side: Impermeable
	Heat flow equation, Eq. (9)	$T = 50^\circ\text{C}$

## 5.2 Verification of the Two-Phase Flow Model

### 5.2.1 Verification Against a Semi-analytical Solution

For the verification, we first need an analytical or semi-analytical solution. Although the [Buckley and Leverett \(1942\)](#) solution is a well-known analytical solution, it cannot be adopted in this verification because it suppresses the capillary drive term and is only suitable for use when externally applied driving forces are large in relation to the gradient of capillary pressure. In common cases, capillary pressure can not be neglected because it has a significant effect on two-phase flow ([Hoteit and Firoozabadi 2008](#)). Until now, although there are still problems in purely analytical approaches, the capillary drive has been considered through numerical solution ([Yortsos and Fokas 1983](#); [Chen 1988](#); [Van Duijn and De Neef 1998](#); [McWhorter and Sunada 1990](#)). Based on [Fučík et al. \(2007\)](#), a semi-analytical solution was obtained for the validation of the new model. Note that, for this verification case, the gravity term is not included. This essentially renders the comparison to be one-dimensional, even though we still simulate the two-phase flow problem on the two-dimensional rectangular domain using the new model. Temperature is constant (50°C). The compression of gas was neglected and the flow rate of gas was set to  $1.0 \times 10^{-5}$  m/s on left injection boundary.

Figure 1 presents the comparison between the semi-analytical model and the new model developed here. In the figure, the simulated water saturation at  $Z = -5$  m is shown as a function of the distance to the CO<sub>2</sub> injection boundary on the left hand side for different times. It can be seen that the simulation slightly underestimates the water saturation in comparison to the semi-analytical solution at the CO<sub>2</sub> front, but in general the agreement can be considered very good. The reason for the above underestimation is that the numerical discretization homogenizes the distribution of water saturation, and leads to an under-prediction of the calculated gradient of water saturation at the front. The extent of underestimation is mainly related to the size of numerical elements and the real gradient of the water saturation. At the CO<sub>2</sub> front, the gradient of water saturation is bigger than in other areas, so the magnitude of under-prediction is bigger here than in other areas when the same size elements are used throughout the domain.

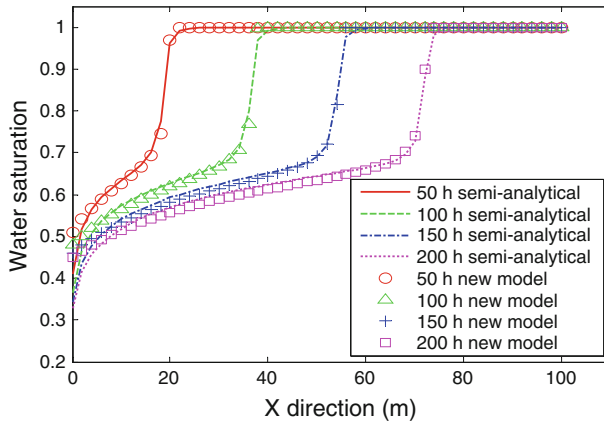


**Fig. 1** Comparison of water saturation as function of distance from the CO<sub>2</sub> source for different times after the start of CO<sub>2</sub> injection, as obtained with the new model and a semi-analytical solution

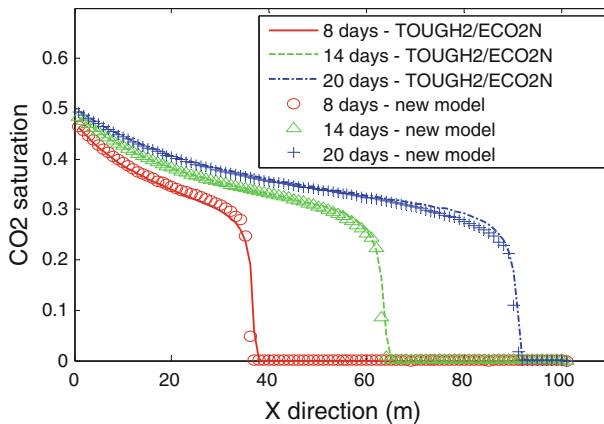


**Fig. 2** Comparison of CO<sub>2</sub> saturation profiles (at  $Z = -5$  m in vertical direction) at different times as simulated using the new model and the numerical model TOUGH2/ECO2N

### 5.2.2 Verification Against TOUGH2/ECO2N

In this simulation, the flow rate of CO<sub>2</sub> was set to  $2.71 \times 10^{-6}$  m/s on left boundary. Temperature is set constant as 50°C (isothermal) for simplicity and convenience of comparison. The numerical mesh used for the computation of TOUGH2/ECO2H has 2,000 elements to ensure precision in these simulations. Figures 2, 3, and 4 show a comparison between the results from the new model and from TOUGH2/ECO2N in terms of simulated gas saturation at different times and as a function of distance from the injection boundary. The general behavior and trends match well, with only slight differences in exact position of the CO<sub>2</sub> front (Fig. 2.). Considering the differences in discretization method and numerical mesh, this small difference is acceptable.

Figures 3 and 4 show the comparison between the spatial distributions of CO<sub>2</sub> saturation simulated with the new model and with TOUGH2/ECO2N at 12 and 20 days after the start of the injection, respectively. The results show a good agreement in most of the model

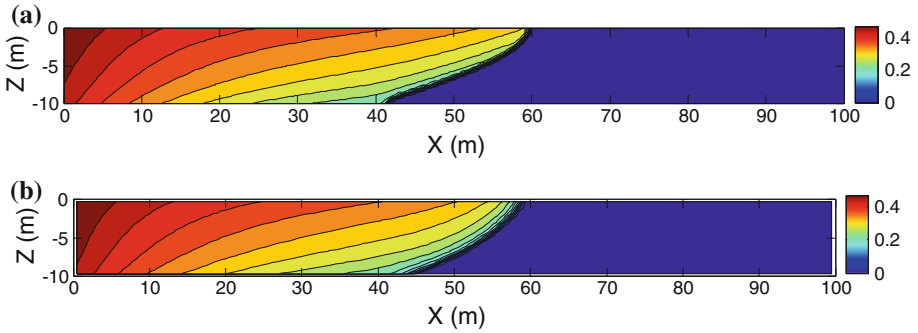


**Fig. 3** The distribution of CO<sub>2</sub> saturation 12 days after the start of the injection as calculated with **a** the new model and **b** with the numerical model TOUGH2/ECO2N

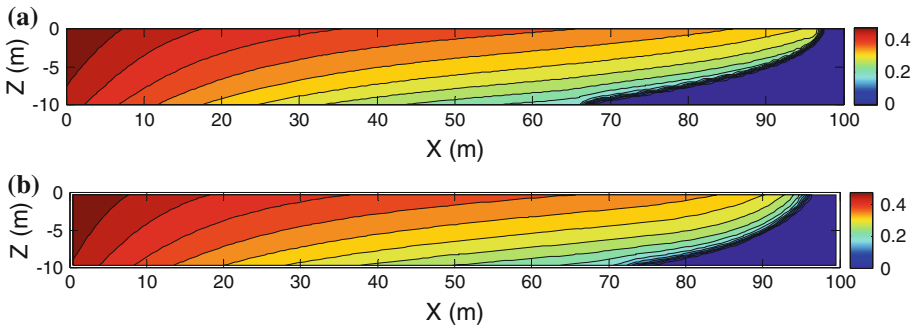


**Fig. 4** The distribution of CO<sub>2</sub> saturation 20 days after the start of the injection as calculated with **a** the new model and **b** with the numerical model TOUGH2/ECO2N

domain, with only differences occurring in the region of the CO<sub>2</sub> front. The main reason for this difference is that different interpolation functions are adopted in the new model and in TOUGH2/ECO2N for the spatial discretization of the governing differential equations. In comparison to the finite volume method (FVM) used in TOUGH2/ECO2N, the finite element method (FEM) adopted in the new numerical model has a higher precision in the regions of large gradient of CO<sub>2</sub> saturation. Thus the gradient of CO<sub>2</sub> saturation simulated by the new model is bigger than that simulated by TOUGH2/ECO2N, in the area of CO<sub>2</sub> front. This indicates that the simulated CO<sub>2</sub> front (interface) is sharper in the new model than in TOUGH2/ECO2N. On the other hand, TOUGH2/ECO2N has a better numerical stability, and the distribution of CO<sub>2</sub> saturation simulated by TOUGH2/ECO2N at the front is smoother than that of the new model.

### 5.3 Verification of the Tracer Transport

Considering that the tracer transport, Eqs. (15) and (16) are similar in form, and same sub-routines were used to solve the two equations in the new FEM code, we only need to verify the solution of one of them. Thus, if the solution of Eq. (15) can be verified, the solution of Eq. (16) will also be verified. For the convenience of comparison, gravity is neglected and the temperature is a constant set as 50 °C. Two special one-dimensional examples are considered in this verification. In the first example, the water flow is ignored, and the flow rate of CO<sub>2</sub> is fixed as constant ( $1.0 \times 10^{-5}$  m/s) everywhere. In this case, the analytical solution

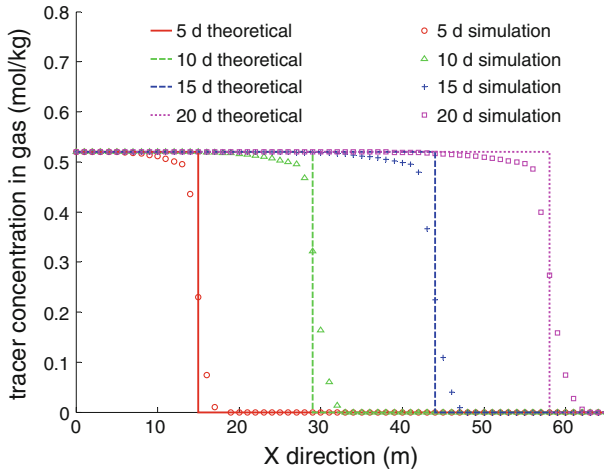


**Fig. 5** Comparison between numerically simulated and analytically determined tracer concentrations for single-phase flow of  $\text{CO}_2$

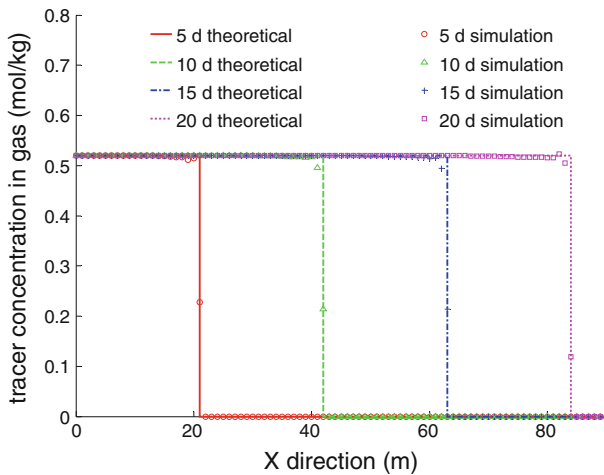


**Fig. 6** Comparison between numerically simulated and analytically determined tracer concentrations for two-phase flow of  $\text{CO}_2$  and brine

can be directly obtained from the time of injection and velocity of  $\text{CO}_2$ . Figure 5 shows the comparison between tracer concentrations as a function of distance and at different times, as simulated with the new numerical model and as determined by the analytical solution. The general agreement is good, with small differences (numerical dispersion) in the region of the front. The reason for these small differences is that the numerical mesh cannot be infinitely dense, and therefore the gradient in the model cannot approach the infinite gradient of tracer concentration at the front.

The second example concerns a two-phase flow simulation. In this calculation,  $\text{CO}_2$  is injected from the left hand side into brine, with a flow rate at the injection boundary being equal to  $2.71 \times 10^{-6}$  m/s. Figure 6 presents the comparison between simulated and analytically determined concentration of tracer in the  $\text{CO}_2$  at different times and as function of

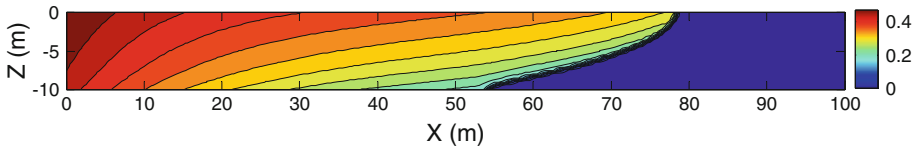


**Fig. 7** The distribution of CO<sub>2</sub> saturation calculated by new model at 16 days

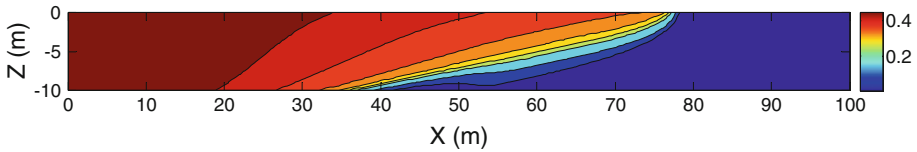


**Fig. 8** The distribution of tracer concentration (mol/kg) in CO<sub>2</sub> calculated by new model at 16 days

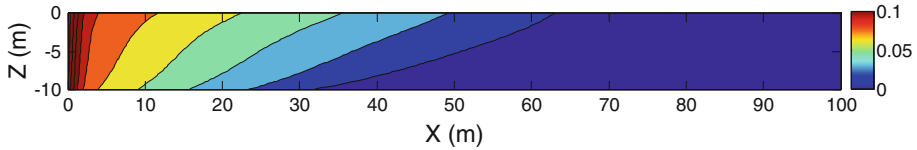
distance from the injection boundary. Again, there is good agreement between simulated and theoretical results. Compared to the first case of single-phase flow, the distribution of tracer concentration in CO<sub>2</sub> matches the analytical solution better in the region of the front. This is because the CO<sub>2</sub> saturation downstream (on the right hand side) of the CO<sub>2</sub> front is equal to 0, and thus the tracer cannot be present in this region.

#### 5.4 Simulation of Tracer Transport in Two-Phase Flow Including Kinetic Transfer of the Tracer

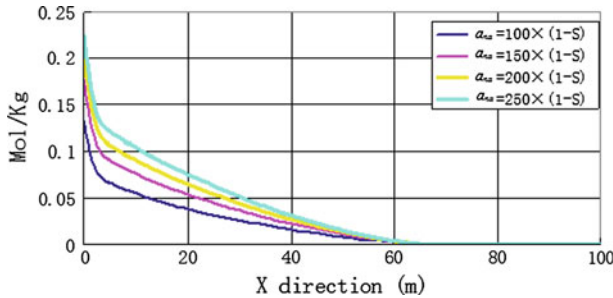
As a whole, it is necessary to present a simulation of tracer transport in two-phase flow, including the tracer transfer from one phase to another. There are, however, no analytical or numerical models that can be used as basis for comparison, so the simulation at this point only provides a demonstration example. Eventually, our objective is to obtain experimental data that will form the basis of a validation. In the present simulation, the injection flow rate of CO<sub>2</sub> is  $2.71 \times 10^{-6}$  m/s. The concentration of tracer in CO<sub>2</sub> on the left hand side injection boundary is 0.52 mol/kg. The initial concentration of tracer in the water is zero. The other computational conditions were defined previously in Sect. 5.1 Based on Grant and Gerhard (2007b); Brusseau et al. (2006), and Miller et al. (1990), the main parameters related to the kinetic mass transfer of tracer between the CO<sub>2</sub> and aqueous phases are set as follows. The average mass transfer coefficient is  $k_1 = 6.8 \times 10^{-7}$ , the total specific interfacial area is  $a_{na} = 154.8 \times (1 - S_1)$ , the pre-exponential factor  $A = 2.02 \times 10^{13}$ , the activation energy  $E_a = 90.0$  and the universal gas constant  $R = 0.008314$ . In this simulation, we focus on advective transport and kinetic transfer of the tracer, thus we have neglected the dispersion effect.

Figure 7 shows the simulated CO<sub>2</sub> saturation at 16 days. The results show that the boundary line of the CO<sub>2</sub>-phase front is slanting up. For a given point in time, the inclination of the boundary line of the CO<sub>2</sub> front mainly depends on the water retention curve and the buoyancy of the CO<sub>2</sub>. The simulated results for tracer concentration in CO<sub>2</sub> and tracer concentration in water at day 16 are shown in Figs. 8 and 9, respectively. Although there are no experimental results yet for comparison, these results indicate that the spatial distributions of tracer obtained with the presented model are realistic, given the preliminary nature of the tracer mass transfer model. Because the velocity of diffusion is far smaller than the velocity of advection, the tracer remains in the region between injection side and the CO<sub>2</sub> front. Simulation shows the





**Fig. 9** The distribution of tracer concentration (mol/kg) in water calculated by new model at 16 days



**Fig. 10** Comparison of simulated tracer concentrations (at  $Z = -5$  m in the vertical direction and at time 20 days) in water for different relationships between specific interfacial area and water saturation

distribution of tracer not only depends on the velocity of  $\text{CO}_2$  flow, but also strongly depends on the rate of tracer mass transfer between the  $\text{CO}_2$  and aqueous phases.

Figure 10 presents a comparison of simulated tracer concentrations in the aqueous phase for different relationships between specific interfacial area and fluid saturation at 20 days. It can be seen that the tracer concentration in the aqueous phase monotonously increases with increasing interfacial area. This is expected because the rate of mass transfer of tracer from the  $\text{CO}_2$  to the aqueous phase is proportional to the interfacial area as described in Eq. (21). Furthermore, the results presented in Fig. 10 show that the distribution of tracer concentration in the aqueous phase is sensitive to changes in interfacial area, which indicates that useful information about the interfacial area can be obtained from tracer data.

## 6 Concluding Remarks

We present a new numerical model of tracer transport in a non-isothermal two-phase flow system of  $\text{CO}_2$  and brine, adding capability to interpret tracer signals including tracers with kinetic/time-dependent interface transfer. The model consists of five different governing equations, describing liquid phase (aqueous) flow, gas ( $\text{CO}_2$ ) flow, heat transport and the movement of the tracers within the two fluid phases, as well as allowing kinetic transport of tracers between the phases. Geochemical reactions and interactions between the dissolved species in the aqueous phase and the solid rock have been incorporated in some two-phase flow codes (e.g., Xu et al. 2004). However, kinetic reactions at the interface between the two fluid phases and kinetic mass transfer over the fluid–fluid interface are features which typically are not available in codes used for  $\text{CO}_2$  storage simulation, and therefore the motivation for the presented model development.

Validation against existing analytical, semi-analytical, and numerical solutions shows good agreement, indicating that the model can simulate non-isothermal two-phase flow and tracer transport with confidence. The numerical model could have been also compared with

similarity solutions of gravity-driven flow under various approximations (e.g., [Huppert and Woods 1995](#); [Nordbotten and Celia 2006](#); [Hesse et al. 2007](#)). However, given that (i) our numerical solution is shown to be in close agreement with those obtained by the widely used and accepted TOUGH2/ECO2N code and (ii) the TOUGH2/ECO2N code has been verified against similarity solutions (see [Pruess 2005](#)), it may not be necessary to perform the verification step with similarity solution for gravity currents.

Although the motivation to develop the model was characterization of geologically stored CO<sub>2</sub> and its phase partitioning and migration in deep saline formations, the model can easily be adapted for other two-phase flow applications, such as NAPL flow and transport.

The solution methodology for the two-phase flow is first to calculate the gas pressure using the equation for conservation of total mass, and then to calculate the water saturation using the gas flow equation. Simulations show that this iterative route is efficient for improving convergence and numerical stability of the two-phase flow calculations, while yet providing accurate results. The Galerkin FEM approach cannot directly be used to solve the tracer transport equations, as artificial and non-physical oscillations will be generated. To overcome this difficulty the weighting functions of a node are set to zero when the gas (or water) pressure of the node is bigger than the gas (or water) pressure of the Gauss integration point. The numerical mesh and the length of the time step also influence the numerical stability and the calculation precision. The numerical results can be further improved if the size of elements can adapt well to the gradient of the primary variables, particularly in the area of wetting front.

The main objective of this work has been to provide a basis for kinetic mass transfer of a tracer between the two fluid phases (the CO<sub>2</sub> and aqueous phases). The presented model further allows incorporation of a chemical reaction involving or producing a tracer at the fluid–fluid interface, thus allowing reaction-controlled kinetic mass transfer from one fluid phase to the other. In a demonstration example, we show that the tracer concentration in the aqueous phase is sensitive to the size of the interfacial area ( $a_{an}$ ) and monotonously increases for increasing  $a_{an}$ . Consequently, a well-designed tracer can provide information about the evolution of the interfacial area over time. Different reactions and kinetic mass transfer models can be chosen and used with the flow and transport model. The mass transfer model presented here is preliminary in nature, as the work continues to find suitable KIS tracers whose specific mass transfer behavior can later be incorporated in our model.

It should be pointed out that the numerical model is not suitable for regimes with viscous instability as discussed in, e.g., [Riaz and Tchelepi \(2006\)](#) and [Riaz et al. \(2007\)](#) or flow with invalidity of volume-averaging (continuum description) as discussed in e.g., [Xu et al. \(1998\)](#) and [Yortsos et al. \(2001\)](#). Finally, non-equilibrium formulations for capillary pressure–interfacial area–saturation (e.g., [Joekar-Niasar et al. 2010](#)) have been proposed in the recent literature. Here, although we have adopted the conventional constitutive relationships (e.g., the van Genuchten model) in the numerical exercises, the numerical model is not limited by these constitutive relationships and it is possible to incorporate the non-equilibrium formulations in our numerical model. However, this is beyond the scope of the current study and motivates further research on this topic. Further work is also underway for continued improvements of the solution technique and additional code verification against laboratory- and field-scale experiments.

**Acknowledgments** The research leading to these results has received funding from the European Community's 7th Framework Programme FP7/2007-2013, under Grant Agreement No. 227286, and from the Swedish Research Council for Environment, Agricultural Sciences and Spatial Planning (FORMAS), Project No. 214-2008-1032. The authors are grateful for fruitful discussions with our MUSTANG project partners.

**Open Access** This article is distributed under the terms of the Creative Commons Attribution License which permits any use, distribution, and reproduction in any medium, provided the original author(s) and the source are credited.

## References

- Allen, M., Isaacson, E.: Numerical Analysis for Applied Science. Wiley, New York (1997)
- Aziz, K., Settari, A.: Petroleum Reservoir Simulation, Environmental Engineering. Elsevier, London (1979)
- Bachmann, J., van der Plog, R.: A review on recent developments in soil water retention theory: interfacial tension and temperature effects. *J. Plant Nutr. Soil Sci.* **165**, 468–478 (2002)
- Baines S.J., Worden R.H.: Geological CO<sub>2</sub> disposal: understanding the long term fate of CO<sub>2</sub> in naturally occurring accumulations. In: Fifth International Conference on Greenhouse Gas Control Technologies, August 13–16, 2000, Cairns, Australia, CSIRO, pp. 311–316 (2001)
- Battistelli, A., Calore, C., Pruess, K.: The simulator TOUGH2/EWASF for modeling geothermal reservoirs with brines and non-condensable gas. *Geothermics* **26**, 437–464 (1997)
- Bear, J., Bachmat, y: Introduction to Modeling of Transport Phenomena in Porous Media. Kluwer, Dordrecht (1991)
- Behrens, H., Ghergut, I., Licha, T., Orzol, J., Sauter, M.: Reactive behaviour of uranine (fluorescein) in a deep geothermal-reservoir tracer test. *Geophys. Res. Abstr.* **8**, 10448 (2006)
- Brooks R., Corey, A.: Hydraulic properties of porous media. Hydrology Paper No. 3. Colorado State University, Fort Collins, CO (1964)
- Brusseau, M.I., Peng, S., Schnaar, G., Costanza-Robinson, M.S.: Relationships among air–water interfacial area, capillary pressure, and water saturation for a sandy porous medium. *Water Resour. Res.* **42**, W03501 (2006)
- Buckley, R.L., Leverett, M.C.: Mechanism of fluid displacement in sands. *Am. Inst. Min. Metall. Pet. Eng.* **146**, 107–116 (1942)
- Chen, Z.X.: Some invariant solutions to two-phase fluid displacement problems including capillary effect. *Soc. Pet. Eng. Reser. Eng.* **3**(2), 691–700 (1988)
- Corey, A.T.: The interrelation between gas and oil relative permeabilities. *Prod. Mon.* **19**, 38–41 (1954)
- Cramer, S.D.: The solubility of methane, carbon dioxide and oxygen in brines from 0° to 300°C. US Bureau of Mines, Report No. 8706, USA, 16pp (1982)
- Fučík, R., Mikyška, J., Beneš, M., Illangasekare, T.H.: An improved semi-analytical solution for verification of numerical models of two-phase flow in porous media. *Vadose Zone J.* **6**, 93–104 (2007)
- Geiger, S., Roberts, S., Matth, S., Zoppou, C., Burri, A.: Combining finite element and finite volume methods for efficient multiphase flow simulations in highly heterogeneous and structurally complex geologic media. *Geofluids* **4**(4), 284–299 (2004)
- Grant, G.P., Gerhard, J.I.: Simulating of dissolution of a complex dense nonaqueous phase liquid source zone: 1. Model to predict interfacial area. *Water Resour. Res.* **43**, W12410 (2007a)
- Grant, G.P., Gerhard, J.I.: Simulating of dissolution of a complex dense nonaqueous phase liquid source zone: 2. Experimental validation of an interfacial area-based mass transfer model. *Water Resour. Res.* **43**, W12409 (2007b)
- Guvanasen, V., Chan, T.: A three-dimensional numerical model for thermohydrromechanical deformation with hysteresis in a fractured rock mass. *Int. J. Rock Mech. Min. Sci.* **37**, 89–106 (2000)
- Helming, R.: Multiphase Flow and Transport Processes in the Subsurface: A Contribution to the Modeling of Hydrosystems. Springer, Berlin (1997)
- Hepple, R.P., Benson, S.M.: Geologic storage of carbon dioxide as a climate change mitigation strategy: performance requirements and the implications of surface seepage. *Environ. Geol.* **47**(4), 576–585 (2004)
- Hesse, M.A., Orr, F.M., Tchelepi, H.A.: Gravity currents in horizontal porous layers: transition from early to late self-similarity. *J. Fluid Mech.* **577**, 363–383 (2007)
- Hoteit, H., Firoozabadi, A.: Numerical modeling of two-phase flow in heterogeneous permeable with different capillarity pressures. *Adv. Water Resour.* **31**, 56–73 (2008)
- Huppert, H., Woods, A.: Gravity-driven flows in porous layers. *J. Fluid Mech.* **292**, 55–69 (1995)
- International Association for the Properties of Water and Steam: IAPWS Release on Surface Tension of Ordinary Water Substance, September (1994)
- Joekar-Niasar, V., Hassanizadeh, S.M., Dahle, H.K.: Non-equilibrium effects in capillarity and interfacial area in two-phase flow: dynamic pore-network modelling. *J. Fluid Mech.* **655**, 38–71 (2010)
- Jury, W.A., Cardner, W.R., Gardner, W.H.: Soil Physics, 5th edn. Wiley, New York (1991)
- Karl, T.R., Trenberth, K.E.: Modern global climate change. *Science* **302**(5651), 1719–1723 (2003)

- Kiehl, J.T., Trenberth, K.E.: Earth's annual global mean energy budget. *Bull. Am. Meteorol. Soc.* **78**(2), 197–208 (1997)
- Li, W.M., Rubin, D., Krempl, E.: *Introduction to Continuum Mechanics*. Pergamon Press, Oxford (1999)
- Licha, T., Sauter, M., Schaffer, M., Maier, F., Nottebohm, M., Fagerlund, F.: Report on batch experiment results for interfacial processes. D041/WP04/MUSTANG (2011)
- McWhorter, D.B., Sunada, D.K.: Exact integral solutions for two-phase flow. *Water Resour. Res.* **26**, 399–413 (1990)
- Miller, C.T., Pirier-McNeill, M.M., Mayer, A.S.: Dissolution of trapped nonaqueous phase liquids: mass transfer characteristics. *Water Resour. Res.* **26**, 2783–2796 (1990)
- Mualem, Y.: A new model for predicting the hydraulic conductivity of unsaturated porous media. *Water Resour. Res.* **12**, 513–522 (1976)
- Niemi, A., et al.: Small-scale CO<sub>2</sub> injection into a deep geological formation at Heletz, Israel. *Energy Proc.* **23**, 504–511 (2012)
- Nordbotten, J.M., Celia, M.A.: Similarity solutions for fluid injection into confined aquifers. *J. Fluid Mech.* **561**, 307–327 (2006)
- Pruess, K.: ECO2N user's guide: a TOUGH2 fluid property module for mixtures of water, NaCl, and CO<sub>2</sub>. Lawrence Berkeley Laboratory Report LBNL-57952, Berkeley, CA (2005)
- Orr Jr, F.M., Stanford, U.: Storage of carbon dioxide in geologic formations. *J. Pet. Technol.* **56**(9), 90–97 (2004)
- Pruess, K., Oldenburg, C., Moridis, G.: Tough2 user's guide version. Lawrence Berkeley Laboratory Report LBNL-57952, Berkeley, CA (1999)
- Pritchett, J.W., Rice, M.H., Riney, T.D.: Equation of state for water–carbon dioxide mixtures: implications for Baca reservoir. Report DOE/ET/27163-8, UC-66a, La Jolla, CA (1981)
- Schaffer, M., Maier, F., Licha, T., Sauter, M.: A new generation of tracers for the characterization of interfacial areas during supercritical carbon dioxide injections into deep saline aquifers: concept for kinetic interface-sensitive tracers (KIS tracer). *Int. J. Greenh. Gas Control.* doi:10.1016/j.ijggc.2013.01.020
- Riaz, A., Tang, G.-Q., Tchelepi, H.A., Kovscek, A.R.: Forced imbibition in natural porous media: Comparison between experiments and continuum models. *Phys. Rev. E* **75**, 011131 (2007)
- Riaz, A., Tchelepi, H.A.: Influence of relative permeability on the stability characteristics of immiscible flow in porous media. *Trans. Porous Media* **64**, 315–338 (2006)
- Stern, S.M., Pitzer, K.S.: An equation of state for carbon dioxide valid from zero to extreme pressures. *Contrib. Min. Pet.* **117**, 362–374 (1994)
- Tomich, J.F., Dalton, R.L., Deans, H.A., Shallenberger, L.K.: Single-well tracer method to measure residual oil saturation. *J. Pet. Technol.* **25**, 211–218 (1973)
- Tong, F.G., Jing, L., Zimmerman, R.W.: A fully coupled thermo-hydro-mechanical model for simulating multiphase flow, deformation and heat transfer in buffer material and rock masses. *Int. J. Rock Mech. Min. Sci.* **47**, 205–217 (2010)
- Tong, F.G., Jing, L., Zimmerman, R.W.: A fully-coupled finite element code for modeling thermo-hydro-mechanical processes in porous geological media. In: *Proceedings 43rd US Rock Mechanics Symposium*, Asheville, NC, USA, 28–30 June 2009
- Tong, F.G., Niemi, A., Yang, Z., Fagerlund, F.: A solution scheme for simulating tracer transport in a non-isothermal two-phase flow system. *Geophysical Research Abstract*, vol. 14, EGU2012-6743-1, EGU General Assembly 2012, Vienna (2012)
- Van Duijn, C., De Neef, M.: Similarity solution for capillary redistribution of two phases in a porous medium with a single discontinuity. *Adv. Water Resour.* **21**(6), 451–461 (1998)
- Van Genuchten, M.Th.: A closed-form equation for predicting the hydraulic conductivity of unsaturated soils. *Soil Sci. Soc. Am. J.* **44**, 892–898 (1980)
- Vargaftik, N.B.: *Tables on thermophysical properties of liquid and gases*, 2nd edn. Wiley, New York (1975)
- Xu, B., Yortsos, Y.C., Salin, D.: Invasion percolation with viscous forces. *Phys. Rev. E* **57**(1), 739–751 (1998)
- Xu, T., Sonnenthal, E., Spycher, N., Pruess, K.: TOUGHREACT user's guide: a simulation program for nonisothermal multiphase reactive geochemical transport in variably saturated geologic media. LBNL Report 55460, V. 1.2., Berkeley, CA, USA (2004)
- Yortsos, Y.C., Xu, B.M., Salin, D.: Delineation of microscale regimes of fully-developed drainage and implications for continuum models. *Comput. Geosci.* **5**(3), 257–278 (2001)
- Yortsos, Y.C., Fokas, A.S.: An analytical solution for linear waterflood including the effects of capillary pressure. *Soc. Pet. Eng. J.* **23**(1), 115–124 (1983)
- Younes, A., Ackerer, P.: Solving the advection–diffusion equation with the Eulerian-Lagrangian localized adjoint method on unstructured meshes and non uniform time stepping. *J. Comput. Phys.* **208**, 384–402 (2005)

- Zhang, Y., Freifeld, B., Finsterle, S., Leahy, M., Ennis-King, J., Paterson, L., Dance, T.: Single-well experimental design for studying residual trapping of supercritical carbon dioxide. *Int. J. Greenh. Gas Control* **5**, 88–98 (2011)
- Zienkiewicz, O.C., Taylor, R.L.: *The Finite Element Method*, vol. 1, Basic Formulations and Linear Problems, 5th edn. Butterworth-Heinemann, London (2000)